

Layer-by-Layer Assembled Multilayers of Polyethylenimine-Stabilized Platinum Nanoparticles and PEDOT:PSS as Anodes for the Methanol Oxidation Reaction

Kyler R. Knowles,[†] Colin C. Hanson,[‡] April L. Fogel,[†] Brian Warhol,[‡] and David A. Rider*,^{†,‡}

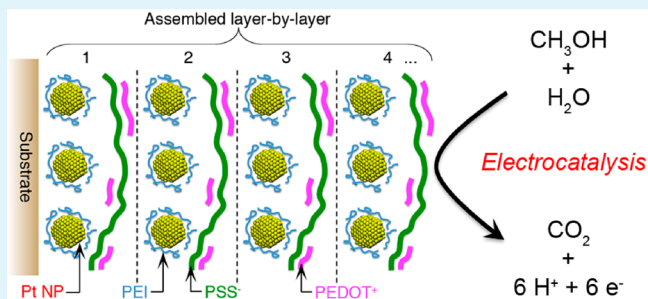
[†]Department of Engineering Technology, Western Washington University, 516 High St., Bellingham, Washington 98225, United States

[‡]Department of Chemistry, Western Washington University, 516 High St., Bellingham, Washington 98225, United States

Supporting Information

ABSTRACT: Polyethylenimine-capped platinum nanoparticles (PEI-capped Pt NPs) are synthesized by photoreduction and qualified as a component for electrostatic layer-by-layer assembly and subsequent electrocatalysis. The PEI-capped Pt NPs are characterized for size and charge using scanning force microscopy, transmission electron microscopy, dynamic light scattering and zetapotential. Well-defined multilayers are produced via thin film electrostatic assembly of PEI-capped Pt NPs with the conducting polymer: poly(3,4-ethylenedioxythiophene):poly(*p*-styrenesulfonate) [(PEI-PEDOT:PSS)⁻Na⁺]. The composite thin films are subsequently characterized by ultraviolet-visible spectroscopy, scanning force microscopy, inductively coupled plasma mass spectroscopy and thermogravimetric analysis. The layer-by-layer deposition process was found to proceed in a controlled manner which permits the fabrication of stable and uniform multilayer thin films. [PEI-capped Pt NPs/(PEDOT:PSS)] multilayers were found to be an active catalyst coating for the oxidation of methanol and a 20 bilayer film proceeds with a stable level of catalyst activity for over 1000 oxidation cycles.

KEYWORDS: *layer-by-layer, multilayer, electrolyte, platinum nanoparticle, polyethylenimine, poly(3,4-ethylenedioxythiophene):poly(*p*-styrenesulfonate), PEDOT:PSS, fuel cell, methanol oxidation, electrocatalysis*



INTRODUCTION

The strategy for creating functional thin films from layer-by-layer assembly^{1,2} has emerged as a robust and versatile technique in numerous fields.^{3–5} Typically, multilayer composite coatings are created from the sequential adsorption of one or more sets of materials with predefined elements for binding and function.^{6–8} Accordingly, functional components capable of hydrogen bonding, van der Waal forces, covalent bonding and electrostatic interactions are often selected as the agents for the assembly of multilayer thin films.^{9–11} By these means, devices applying functional multilayer coatings with roles in energy conversion, sensing, drug-release, lithography, electronic signalling and memory, biological function, and catalysis have been created.^{12–20} In particular, nanoparticle multilayer coatings have emerged as candidates for fuel cell technology given the ease of fabrication, the high degree of control and tunability of the material properties of the multilayer and the nanoscale precision in the architecture of the coating.²¹ Conceptually, a multilayer architecture is attractive for fuel cell catalyst layers in that a host matrix material is introduced and is in intimate contact with catalyst particles and may impart tailored fuel permeability, manage solvent migration and reduced catalyst particle diffusion.^{22–24}

Direct methanol fuel cells (DMFCs) are attractive portable power devices for the conversion of chemical energy into electrical energy.^{25–27} The relatively high energy efficiency, high power density, low operating temperatures and low level of pollutant by-products of the technology are features that advocate for its widespread integration into future energy systems. To date however, the deployment of a DMFC-based infrastructure had been largely hindered by high cost and modest performance. In the former, DMFCs generally rely on the use of platinum as a catalyst for executing the reduction and oxidation reactions and, due to the high cost associated with this rare metal, is often the most expensive component of the fuel cell.^{28–30} In the latter, the crossover of methanol fuel from the anode to the cathode contributes to the sub-optimal performance of a DMFC.^{31–33} Moreover, the blocking of catalyst surface sites by undesirable oxidation by-products of the methanol oxidation reaction further diminishes electrode activity and often compromises the power output for the device.³⁴ Consequently, there is a need for a methodology for

Received: April 12, 2012

Accepted: June 25, 2012

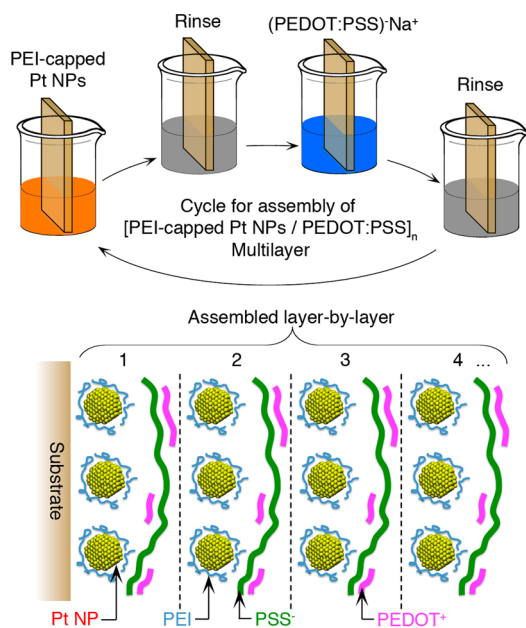
Published: June 25, 2012



creating robust catalytic Pt layers in an inexpensive manner from stable and environmentally friendly solvents. The strategy of layer-by-layer deposition of polyelectrolyte layers for fuel cells has emerged recently and has in part managed methanol crossover in some systems.^{12,34,35} Currently, the fabrication of multilayers containing robust nanoparticle catalysts for DMFCs is less-well explored.^{21,22,36-42}

In this work, we investigate the applicability of polyethylenimine-capped platinum nanoparticles as a water-dispersible cationic component for layer-by-layer assembly. To favor electrocatalytic function we therefore further defined our study to include assembly with the aqueous and anionic conducting polymer couple poly(3,4-ethylenedioxythiophene):poly(*p*-styrenesulfonate) [(PEDOT:PSS)⁻Na⁺] to act as a conducting compliment component in the coating.^{33,43,44} We present herein: (i) the synthesis of the cationic and water dispersed polyethylenimine-capped platinum nanoparticles, (ii) an investigation into the layer-by-layer deposition and nanostructure of multilayers of PEI-capped Pt NPs and (PEDOT:PSS)⁻Na⁺ (see Scheme 1), and (iii) the catalytic activity and stability of the multilayer nanocomposite thin films for the methanol oxidation reaction.

Scheme 1. Schematic for the LbL Assembly of PEI-Capped Pt NPs with (PEDOT:PSS)⁻Na⁺ (top) and an Illustration Depicting the Cross-Section of a [PEI-Capped Pt NP / (PEDOT:PSS)⁻Na⁺]_n Multilayer (Below) Showing the Components Deposited in Each Bilayer (Separated by Dashed Boundaries)^a



^aThe illustration does not reflect the exact morphology in the multilayer.

EXPERIMENTAL SECTION

Materials and General Instrumentation. Polyethylenimine (PEI, 50 wt % aqueous solution, average molecular weight 50 kDa) and hexachloroplatinic acid ($H_2PtCl_6 \cdot 6H_2O$) were used as received from Sigma Aldrich. Because of the polydispersity of synthetic macromolecules such as PEI, the convention used herein to express the concentration of aqueous PEI solutions is reported in terms of the monomer residue molar concentration. The generalized monomer

residue in PEI is $-\text{CH}_2-\text{CH}_2-\text{NH}-$ with formula weight 43 Da, and as an example, a PEI solution of 4.3 mg/mL is therefore reported as 0.1 M in monomer residue molar concentration.

A commercially available colloidal suspension of poly(3,4-ethylenedioxythiophene):poly(*p*-styrenesulfonate) [(PEDOT:PSS)⁻Na⁺] was used as received from Heraeus (Clevios P VP Al 4083). Silicon wafer, quartz glass and indium tin oxide glass substrates ($8-12 \Omega/\text{square}$) were acquired from Nova Electronic Materials, Chemglass Inc. and Delta Technologies, respectively. The substrates were cleaned by sequential rinsing in dichloromethane, ultrapure water ($18 \text{ M}\Omega$) and isopropyl alcohol, and were further cleaned by exposure to a 10 min argon plasma at $\sim 0.1 \text{ Torr}$ (Harrick Plasma, PDC 32G, 18W) immediately prior to use. Similarly, coatings supported on these substrates were reactive ion etched using this equipment and this procedure.

UV-photoreduction was carried out with a Rayonet photochemical reactor (model RPR-600, Southern New England Ultraviolet Inc.) equipped with eight 253.7 nm light sources, each at a power of 8W. Samples were spin coated at 3 krpm for 60 sec using a WS-400B-6NPP Lite Laurell Spin Coater. Optical microscopy and absorption spectroscopy were performed using an Olympus BX50 optical microscope and Jasco V670 UV-Vis Spectrophotometer, respectively. Scanning force microscopy (SFM) was conducted using a digital Instrument Nanoscope IIIa multimode instrument operated in tapping mode and equipped with conical tapping mode silicon probes (Nanoscience Instruments) with resonant frequencies close to 300 kHz. Transmission electron microscopy (TEM) was performed using Hitachi 8100 scanning transmission electron microscope with an accelerating voltage of 200 keV. After drying samples at 100°C for a minimum of 4 h, thermogravimetric analysis (TGA) was executed with a TA Instruments TGA Q-500 equipped with a nitrogen purged furnace operated a heating rate of $10^\circ\text{C}/\text{min}$.

Zeta potential measurements were performed using a Zetasizer Nano-ZS (Malvern Instruments Ltd, Westborough, MA) whereas dynamic light scattering (DLS) measurements were conducted using Delsa Nano S (Beckman Coulter, Inc., Fullerton, CA) equipped with a 658 nm laser diode and an automatically controlled photomultiplier and aperture attenuator set to collect scattered light at an angle of 15° with a photon counting rate of ca. 10 kcps. Prior to the measurements, polymer and NP solutions were filtered through Millipore syringe filters ($0.45 \mu\text{m}$ pore size). Size measurements were made on $\sim 1 \text{ mL}$ of sample in a disposable cuvette (1 mL capacity) using ultrapure water as solvent ($n = 1.3329$, $\eta = 0.890 \text{ cP}$ at $25 \pm 1^\circ\text{C}$). The samples were allowed to equilibrate at 25°C for ~ 15 minutes before each measurement, followed by a 60 s acquisition time (1 s per acquisition). The calculation of the particle size and size distribution was performed using CONTIN particle size analysis routines. The intensity, volume and number distributions plots were averaged and the data is reported as the average diameter of the particles.

Element-specific detection was carried out using an inductively coupled plasma mass spectrometer (ICP-MS; Agilent 7500 CE, Palo Alto, CA) equipped with an octopole reaction system, a 193 nm laser ablation system UP213 (New Wave Research, Fremont, CA) and an automated peristaltic pump operated at 0.5 rps. The optimized conditions used for ICP-MS measurements are listed in Supporting Information Table S1. Briefly, samples were arranged in a laser ablation chamber (Supercell, New Wave Research, Fremont, CA) and ablated under identical experimental conditions, in order to allow the calculation of the relative ^{34}S and ^{195}Pt isotopic signal. The ablated material was transported by helium carrier gas to the plasma torch. The ICP-MS instrument tuning was optimized with respect to the maximum ion intensity of low masses. The carrier gas flow rate was adjusted to optimize the output signal.

Synthesis of PEI-Capped Platinum Nanoparticles. The synthesis of PEI-capped platinum nanoparticles (PEI-capped Pt NPs) follows a modified protocol as outlined by Bai et al.⁴⁵ In brief, 1 mL of 10 mM hexachloroplatinic acid ($H_2PtCl_6 \cdot 6H_2O$) was added to 8.49 mL of a 20 mM PEI aqueous solution and subsequently further diluted with 7.16 mL of water ($18 \text{ M}\Omega$) and stirred for one hour. The faint yellow solution was then transferred to a quartz reactor cell and

Table 1. Summary of Hydrodynamic Diameter, Polydispersity (PD), and pH for Aqueous Solutions of PEI, H_2PtCl_6 -Loaded PEI, PEI-Capped Pt NPs, and $(\text{PEDOT:PSS})^-\text{Na}^+$

component	hydrodynamic diameter, D_h , in nm (PD)	pH of solution (conc.)	zeta potential in mV
PEI	112 (0.295)	8.2 (10 mM PEI)	+29
H_2PtCl_6 -loaded PEI	320 (0.083)	6.5 (0.6 mM H_2PtCl_6 ; 10 mM PEI)	+58
PEI-capped Pt NPs	205 (1.002)	6.1 (10 mM PEI)	+47
$(\text{PEDOT:PSS})^-\text{Na}^+$	182 (0.732)	2.5 (0.03–0.04 g/L ^a)	-46

^aBased on percent solid content from product information and 1:3 v/v aqueous dilution of $(\text{PEDOT:PSS})^-\text{Na}^+$ with water (18 MΩ).

exposed to UV-irradiation for 24 h, which caused the solution to become a faint brown color. UV-Vis absorption spectroscopy and dynamic light scattering were used to monitor the photoreduction of the H_2PtCl_6 and the change in particle size, respectively.

Layer-by-Layer (LbL) Assembly. Layer-by-layer deposition was performed manually. Freshly cleaned silicon wafer, quartz or ITO substrates (bearing a native negatively charged surface)¹ were immersed in PEI-capped Pt NP solutions for 3 min, removed and rinsed with copious amounts of water. The substrates were then immersed in a 1:3 v/v aqueous solution of $(\text{PEDOT:PSS})^-\text{Na}^+$ in ultrapure water (18 MΩ) for 3 min and rinsed with water to complete a deposition cycle for a single bilayer. This cycle was repeated until the desired number of bilayers was achieved.

Electrochemical Analysis. Cyclic voltammetry was carried out either using a Parstat 2273 or a EG&G Model 283 potentiostat employing a standard three-electrode electrochemical cell. All potentials are reported relative to a Ag/AgCl reference electrode recorded at a scan rate of 0.050 V/s. Experiments were carried out at room temperature in degassed 0.1 M H_2SO_4 and 2.0 M MeOH aqueous solution. The counter electrode was platinum wire and the working electrode consisted of an ITO electrode bearing the film of interest.

RESULTS AND DISCUSSION

Synthesis and Characterization of PEI-Capped Platinum Nanoparticles. The method selected for creating water-dispersible cationic platinum nanoparticles (Pt NPs) is based on the photoreduction of aqueous hexachloroplatinic acid in the presence of the polymeric ligand, polyethylenimine (PEI). Recently, Bai et al. have shown that water-dispersible Pt NPs could be synthesized by this method and that UV-crosslinked material was active for methanol oxidation.⁴⁵ The PEI ligand, comprised of primary, secondary, and tertiary aliphatic amine groups in a ratio of approximately 1:2:1,⁴⁶ is a polyelectrolyte with a pH-tunable charge density that allows for adjusting the rate of film growth in layer-by-layer deposition.^{47–49} In this capacity, a PEI-capped Pt NP represents an excellent candidate for a layer-by-layer assembly approach for creating catalytically active thin films.⁵⁰

Absorption spectroscopy, dynamic light scattering and zetapotential can be used to monitor the formation of PEI-capped Pt NPs in solution. A summary of the evolution of the solution pH, particle size and charge is reported in Table 1. Prior to loading the PEI with acidic H_2PtCl_6 , the hydrodynamic diameter (D_h) of PEI at pH 8.2 was found to be 112 nm. After introduction of H_2PtCl_6 , the D_h increased to 320 nm with concomitant change in the solution pH to 6.5. This increase in D_h can be attributed to several contributing phenomenon including the protonation of the amine residues in PEI and subsequent chain elongation due to intramolecular electrostatic repulsion as well as a complex coordination at Pt centers where cross-linking several PEI chains results.⁵¹ Supporting this mechanism was the observation of an increase in the zetapotential value for the PEI upon loading with H_2PtCl_6 from +29 mV to +58 mV. Upon UV-irradiation of an aqueous

solution of H_2PtCl_6 and PEI with 254 nm light for 24 h, solutions were observed to undergo a color change from yellow to brown.⁴⁵ The disappearance of the ligand-to-metal charge transfer peak in the UV-Vis spectra at 235 nm and a concomitant increase in the baseline absorption of exposed solutions confirmed photoreduction of Pt(IV) to Pt(0) NPs (see Supporting Information).⁵² Following photoreduction, the D_h value for PEI-capped Pt NPs in solution was 205 nm, while the pH of the solution was modified to 6.1. In this case, the decrease in D_h is likely attributed to a combination of chain cleavage due to oxidation of PEI chains and a coalescence of many Pt(0) centers to form NPs. This type of modification of the PEI is reflected in the decreased level of positive charge on the modified PEI (zeta potential value of +47 mV). We propose that the change in pH is due to PEI cleavage at the more basic tertiary aliphatic amine groups or that these tertiary amines are modified by the Pt NP surface and therefore render them less basic and consequently modify the solution acidity level. Nonetheless, the light-scattering and zetapotential measurements have qualified the PEI-capped Pt NPs as a positively-charged candidate that is appropriate for LbL assembly.

The PEI-capped Pt NPs were characterized in the solid state by scanning force microscopy (SFM), transmission electron microscopy (TEM) and selected area electron diffraction (SAED). Solutions of PEI and PEI-capped Pt NPs were spin coated onto clean Si wafer substrates and investigated by SFM (see Figure 1a–d). The thin film fabricated from PEI-capped Pt NPs depicted an interesting morphology in the height mode SFM channel (Figure 1b). Isolated and well-defined Pt NPs with an approximate diameter of 15 nm were resolved from a continuous supporting matrix of PEI. To confirm the assignment of this morphology, a thin film control sample of H_2PtCl_6 -loaded PEI was also studied. In this case, the film depicted an essentially featureless topography, which confirms that the particles found in Figure 1b are only generated after a 24 h UV exposure. This assignment is further reinforced by characterizing films transformed by a reactive ion etch procedure using Ar plasma. Given that PEI is readily degraded to carbonaceous by-products during the etch procedure, any existing inorganic Pt NP would be expected to remain largely unaltered and therefore identified as metallic in composition. Similarly, the H_2PtCl_6 -loaded PEI sample, which lacks preformed Pt NPs, would be expected to afford a largely featureless film (where any remaining Pt would create a background blanket Pt layer). Shown in Figure 1c and 1d are the resulting SFM images of the etched films created from solutions of H_2PtCl_6 -loaded PEI and PEI-capped Pt NPs, respectively. An essentially featureless SFM image was found for the former whereas the corresponding etched film from PEI-capped Pt NPs clearly revealed isolated Pt NPs reminiscent of those described in Figure 1b. The average height of the isolated Pt NPs was found to be ~11 nm, a diameter value that correlates with previous work for the synthesis of Pt NPs by

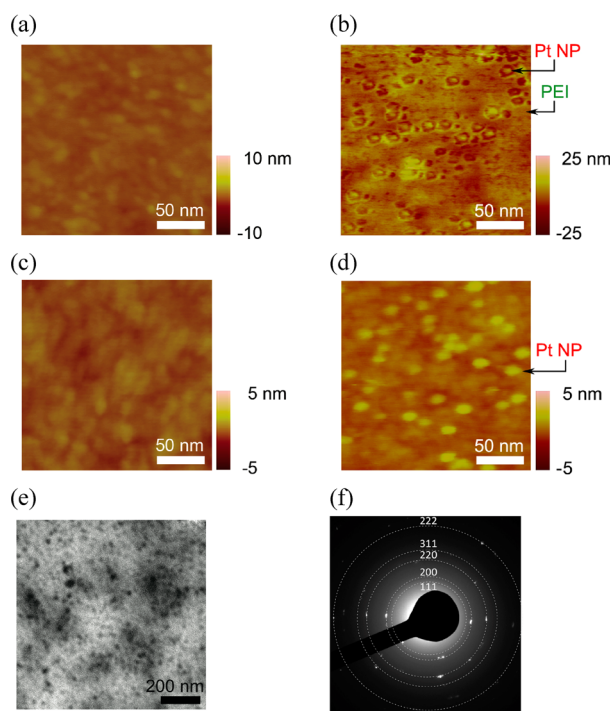


Figure 1. SFM height images for (a) H_2PtCl_6 -loaded PEI and (b) PEI-capped Pt NPs spin-cast onto a silicon substrate. SFM height images for Ar plasma etched (c) H_2PtCl_6 -loaded PEI and (d) PEI-capped Pt NPs films. (e–f) TEM image and SAED of PEI-capped Pt NPs with superimposed rings indexed to FCC Pt to guide the eye.

photoreduction.⁴⁵ Importantly, this SFM estimation for the size of Pt NPs suggests that these structures would be catalytically active for methanol oxidation.⁵³

The structural conclusions gleaned from TEM observations of the PEI-capped Pt NPs largely align with those established in the SFM study. Shown in Figure 1e is a representative TEM image of PEI-capped Pt NPs. Isolated and well-defined Pt NPs are resolved, where the TEM-estimated average diameter of the NPs was found to be 14 nm, a value that closely matches that found by SFM and previous literature.⁵⁴ This characterization further reinforces the assignment of the morphology found in the corresponding film reported in Figure 1b. Crystallinity was qualified in the Pt NPs by SAED and is presented in Figure 1f. A pattern consistent with nanocrystalline platinum metal emerged where the high intensity spots were indexed to several diffraction planes for face-centered cubic (FCC) platinum. Diffraction spots coincident on five of these superimposed

index rings were found to correspond to the (111), (220), (220), (311), and (222) planes of a crystalline FCC Pt.⁵⁵

Electrostatic Layer-by-Layer Assembly of PEI-capped Pt NPs with (PEDOT:PSS)[−] Na^+ . The PEI-capped Pt NPs are stabilized with a ligand consisting of primary, secondary and tertiary amine residues that impart cationic charge to the particle. Coupling this material with an anionic polyelectrolyte would consequently permit electrostatic binding of the two components in a multilayer film. Poly(3,4-ethylenedioxythiophene):poly(*p*-styrenesulfonate) [(PEDOT:PSS)[−] Na^+] is a polymer blend of cationic and conducting PEDOT⁺ that is charge-balanced by anionic PSS[−] Na^+ . The strongly coupled (PEDOT:PSS)[−] is rich in PSS[−] Na^+ with a PEDOT:PSS[−] Na^+ ratio of approximately 1:6 and hence bares an overall negative charge in aqueous solution.⁵⁶ The layer-by-layer (LbL) assembly of (PEDOT:PSS)[−] Na^+ as an anionic polymer component partnered with various cationic materials has recently been explored.^{53,56–58} To confirm the required electrostatic binding between PEI-capped Pt NPs and (PEDOT:PSS)[−], samples of the two solutions were mixed and observed with an optical microscope. Upon mixing, the formation of a precipitate was observed indicating strong attraction between the two components and the formation of an extended macromolecular network that is no longer soluble.⁵⁹

The LbL assembly of PEI-capped Pt NPs with (PEDOT:PSS)[−] Na^+ requires a charged substrate and is executed with iterations of the cycle depicted in Scheme 1. Freshly cleaned quartz or ITO substrates bear negatively charged oxide surfaces and are useful substrates for monitoring the assembly process and electrochemical activity of the resulting multilayers, respectively (vide infra). Immersion of the substrate of choice into an aqueous solution of positively charged PEI-capped Pt NPs permits the electrostatic binding of this to the surface of the substrate and, due to charge over-compensation by the PEI for the surface charges, the sample surface is rendered positive in charge. Subsequent immersion into an aqueous solution of (PEDOT:PSS)[−] Na^+ binds this complement material by way of negatively charged sulfonate residues on the PSS[−] and, by an analogous mechanism, reverses the overall charge of the sample surface back to a negative state. At this point, the fabrication sequence has generated the first complete bilayer of the two materials and for nomenclature purposes is defined as [PEI-capped Pt NP/(PEDOT:PSS)]_n where $n = 1$. Accordingly, repetition of the fabrication cycle n times leads to a multilayer with n bilayers. An illustrative depiction of the cross-section multilayer coating is shown at bottom in Scheme 1 where adjacent bilayers are distinguished by dashed lines. This

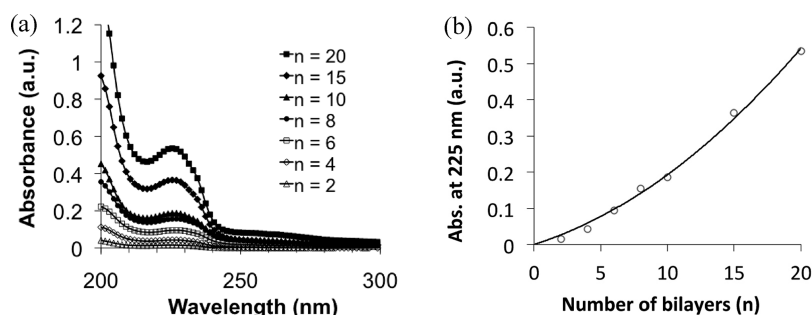


Figure 2. (a) Selected UV–vis spectra of [PEI-capped Pt NPs/(PEDOT:PSS)]_n multilayers with a bilayer range $n = 2–20$ fabricated on a quartz substrate. (b) Plot for absorbance value at 225 nm vs bilayer number (n) for [PEI-capped Pt NPs/(PEDOT:PSS)]_n multilayer series described in a.

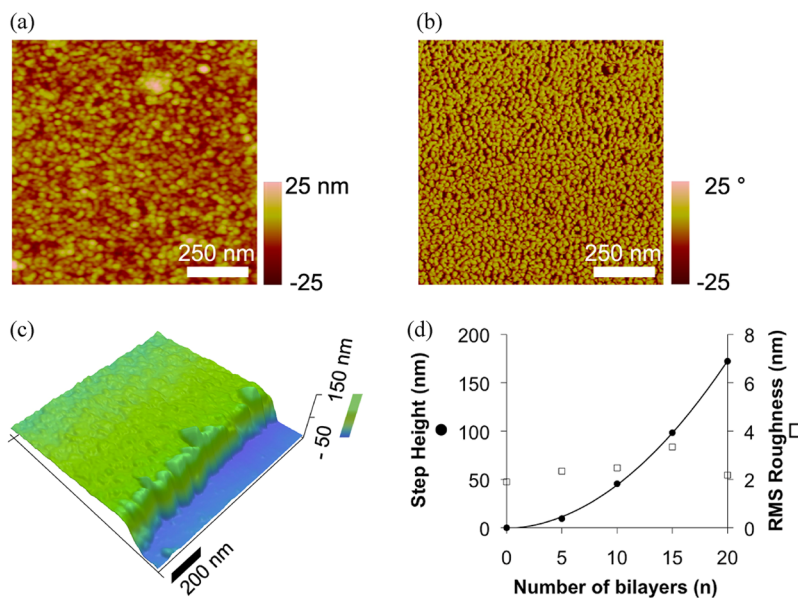


Figure 3. SFM height (a) and phase (b) images for the surface of $[\text{PEI-capped Pt NPs}/(\text{PEDOT:PSS})]_{10}$. (c) SFM height image for a step height feature for thin films of $[\text{PEI-capped Pt NPs}/(\text{PEDOT:PSS})]_{15}$. (d) Plot for step height and RMS roughness vs. bilayer number for $[\text{PEI-capped Pt NPs}/(\text{PEDOT:PSS})]_n$ multilayer films on quartz with a bilayer range $n = 0\text{--}20$.

ordered representation however likely does not reflect the true morphology of the multilayer as LbL coatings have been shown to consist of a disordered architecture of interpenetrating networks of each component.

Characterization of LbL Growth by Absorption Spectroscopy. The LbL fabrication of a $[\text{PEI-capped Pt NP}/(\text{PEDOT:PSS})]_n$ multilayer is accompanied with a corresponding increase in the optical density of the sample. Characterization of the progress of the LbL coating procedure was conducted by UV-vis spectroscopy on quartz-supported multilayers. Shown in Figure 2a are the absorption spectra for a series of multilayers. Due to the high optical transparency of both components in the visible light range, only the UV range is presented in the plot. A characteristic peak at $\lambda_{\text{max}} = 225 \text{ nm}$ was discernable in all spectra which can be attributed to the $\pi\text{--}\pi^*$ transition for $(\text{PEDOT:PSS})^-$ (see Supporting Information). As the bilayer number increases, the absorption value for this feature was also found to increase. Shown in Figure 2b is a plot created from the absorbance value for the $\lambda_{\pi\text{--}\pi^*}$ versus bilayer number and depicts a trend that can be fit to a second order polynomial. The predictable increase in this absorption feature is a testament to the high level of control in this LbL coating strategy. This nonlinear growth mode implies that a reversible interdiffusion of PEI-capped Pt NPs and PEDOT:PSS⁻ occurs during the deposition sequence.^{60,61} Previous research on the LbL assembly of PEI with various polyanions has also shown that the pH level of the solution can select for this nonlinear growth mechanism.^{47\text{--}49,62,63}

SFM Study of the Surface Structure and Film Thickness. To assess the uniformity and surface structure of the $[\text{PEI-capped Pt NPs}/(\text{PEDOT:PSS})]_n$ multilayer coatings, tapping mode SFM was performed on films created on quartz or ITO substrates. A set of representative height mode and phase mode SFM images of the surface of a $[\text{PEI-capped Pt NPs}/(\text{PEDOT:PSS})]_{10}$ multilayer is reported in Figure 3a and 3b, respectively. As represented in Figure 3a, the surface of the multilayer coatings consists of a high density of particle-like features with very uniform size and topography. The SFM

estimated diameter of these features is $\sim 12 \text{ nm}$, a value that closely matches the size of features described in Figure 1. This measurement therefore confirms that the PEI-capped Pt NPs have been successfully included into the multilayer coating. Further confirmation for this assignment arises when examining the corresponding phase mode image where all these features are more easily resolved from the surrounding matrix. Similar topographies were found for multilayers on both quartz and ITO substrates for a range of bilayer numbers $n = 5\text{--}20$. The consistency in the surface topography across the entire multilayer series confirms a well-controlled coating procedure.

To further characterize the quality and thickness of the multilayer coatings, a step height analysis was conducted on quartz supported films bearing a physically removed portion. A height SFM image of such an area is depicted in Figure 3c for $[\text{PEI-capped Pt NPs}/(\text{PEDOT:PSS})]_{15}$. A clear and well-defined step transition in topography was found that distinguishes the multilayer film (green region in Figure 3c) from the exposed quartz substrate (blue region in Figure 3c). Using step-height analysis of the image, an estimate of the film thickness is made and in this case was determined to be 97 nm. Figure 3d summarizes the analogous step-height values for $[\text{PEI-capped Pt NPs}/(\text{PEDOT:PSS})]_n$ for the bilayer range of $n = 0\text{--}20$. The thickness of the multilayer increases with bilayer number according to a second-order polynomial trend, which agrees with the aforementioned optical density trend for the same series. Noteworthy is the relatively low roughness of the surfaces of the multilayers. Figure 3d also summarizes the RMS roughness values determined from $3 \mu\text{m}^2$ height SFM images for the same bilayer number range. In all cases, the roughness values were $\sim 2\text{--}4 \text{ nm}$, a measure that closely matches the inherent roughness of the pristine substrate (in this case, quartz).

Composition of the LbL Assembled Multilayers. To confirm the presence of the Pt NPs and the PEDOT conductive element in the multilayers, a series of films were studied by inductively coupled plasma mass spectroscopy (ICP-MS) and thermogravimetric analysis (TGA). Laser ablation

ICP-MS resolved Pt-loading bilayer-by-bilayer and determined that the relative atomic concentrations of Pt and S approach $\sim 0.07\%$ and $\sim 0.02\%$, respectively. By applying earlier film thickness data and an analysis of nitric acid digested films, it was determined that as higher bilayer number films are targeted, the Pt-loading approaches 1.3 mg/cm^3 (see Supporting Information for ICP-MS analyses). This relatively low Pt-loading is attributed to several factors including an initial low Pt-loading in the PEI, possible desorption with ongoing multilayer deposition or, as observed in other similar Pt NP LbL assembled films,⁴² a decrease in the charge density of PEI-capped Pt NP deposition. Strategies for increasing the Pt-loading include chemical reduction of Pt metal ion after multilayer film deposition⁴² and reduced rinsing during the deposition cycle.²² TGA was used to estimate the inorganic content of a $[\text{PEI-capped Pt NPs}/(\text{PEDOT:PSS})]_{20}$ film heated to 900°C . The mass yield was then compared to those of the corresponding by-products isolated from the constituent parent polymer materials, namely PEI and $(\text{PEDOT:PSS})^-\text{Na}^+$. Shown in Figure 4 are the resulting

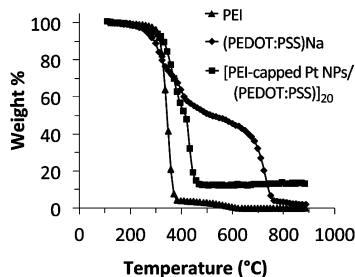


Figure 4. TGA plots for (i) PEI, (ii) $(\text{PEDOT:PSS})^-\text{Na}^+$, and (iii) a $[\text{PEI-capped Pt NPs}/(\text{PEDOT:PSS})]_{20}$ multilayer.

thermograms for the study. Inspection of the data reveals that after heating $(\text{PEDOT:PSS})^-\text{Na}^+$ above 800°C , most volatile by-products are evolved and that $\sim 2 \text{ wt \%}$ of the sample remains. The corresponding trace for the PEI showed near-complete evolution of the material leaving only 0.1 wt \% as a by-product. The thermogram for the $n = 20$ sample revealed a significant difference from its constituent materials. A relatively stable non-combustible inorganic material was isolated at $\sim 475^\circ\text{C}$ with a corresponding mass yield of $\sim 12 \text{ wt \%}$. An estimate for Pt NP particle density can be calculated if the mass yield is assumed to arise from platinum loading alone and that the density of the PEI/PEDOT:PSS matrix is assumed to be in the range of that of the starting polymers (1.50 and 1.05 g/cm^3 , respectively;⁶⁴ see Supporting Information). Given that the average Pt NP diameter found by SFM was 11 nm (see above) and that this film was 172 nm thick (see Figure 3d), the number density of Pt NPs present in the $[\text{PEI-capped Pt NPs}/(\text{PEDOT:PSS})]_{20}$ is estimated to be $\sim 8000\text{--}11\,000 \text{ per } \mu\text{m}^3$.

Catalysis Using [PEI-Capped Pt NPs]/(PEDOT:PSS)]₃₀. The electrocatalytic activity of the Pt NPs within the multilayers for the methanol oxidation reaction was studied by cyclic voltammetry.⁶⁵ To assist in the assessment of this activity, an additional control multilayer representing the polymeric matrix was fabricated from pristine PEI and characterized in the same manner. In either case, the multilayers were not thermally activated beforehand. Shown in Figure 5a are the voltammograms recorded using $[\text{PEI}/(\text{PEDOT:PSS})]_{20}$ and $[\text{PEI-capped Pt NPs}/(\text{PEDOT:PSS})]_{20}$ (coated on an ITO electrode) in aqueous 0.1 M sulphuric acid

and 2 M methanol. The voltammogram for the control sample depicted an essentially featureless trace largely dominated by a wide capacitance cycle that is typical for a PEDOT:PSS composite.⁶⁶ Interestingly, the voltammogram for the $[\text{PEI-capped Pt NPs}/(\text{PEDOT:PSS})]_{20}$ electrode depicted a similar background signal with an important difference: an anodic peak at 0.65 V . This peak, indicative of a complex methanol oxidation mechanism, is defined by a low-overpotential region $E < 0.65 \text{ V}$, where methanol adsorption and dehydrogenation occurs to produce Pt-adsorbed CO and at $E \approx 0.65 \text{ V}$, a subsequent process for reaction with surface tethered water to produce CO_2 .^{36,67,68} Previous research on multilayers containing Pt NPs capped by the similar poly(amidoamine) dendrimer ligand has found these same characteristics for the methanol oxidation reaction.⁶⁹ Film thickness and Pt-mass loading measurements allow for a comparison of the electrocatalytic activity across a series of multilayer films defined by $n = 5, 10, 15$, and 20 (see Supporting Information for CV plots normalized for multilayer thickness and Pt-loading). Shown in Figure 5b is data found for the peak current and onset potential for the methanol oxidation reaction plotted against the bilayer number. A maximum catalytic activity of 91 A/g was found for the $n = 10$ bilayer film while the onset potential was found to decrease as the bilayer number, n , increased. The catalytic activity of the $n = 10$ bilayer film is $\sim 20\%$ higher than that of a typical commercial catalyst (E-TEK 40% Pt@Vulcan XC-72)⁷⁰ and consistent with other recently investigated carbon-supported Pt NPs systems.^{71,72}

To assess the longevity of the catalytic activity of the $[\text{PEI-capped Pt NPs}/(\text{PEDOT:PSS})]_{20}$ multilayer, the electrochemistry study was expanded to include 4800 electrocatalytic cycles where the potential of the multilayer electrode was repeatedly ramped between 0 and 1 V (vs Ag/AgCl) at 0.050 V/s with an intermittent 2 s resting interval at 0 V between each cycle. During much of the course of the experiment, the peak current density of the forward scan anodic peak for methanol oxidation was found to be near constant indicating a relatively constant electrocatalytic activity (See Figure 5c for selected voltammograms). Figure 5d reinforces this observation by plotting the anodic peak current density value versus the logarithm of the voltammogram cycle number and reveals that the multilayer maintains a constant catalytic activity for up to ~ 1100 cycles of the methanol oxidation reaction. The mechanism for the decreased activity is undetermined however negative contributions from leaching or electrochemical etching of the Pt NPs and breakdown of the ITO substrate are possible contributing factors and represent the focus of current research. At this point, the prolonged level of activity towards the methanol oxidation reaction is proposed to result from a constant electrocatalytically active surface area for Pt by way of reduced NP particle diffusion and aggregation within the multilayer or a possible resiliency to CO poisoning.⁷³ Detailed chemical and physical analysis of $[\text{PEI-capped Pt NPs}/(\text{PEDOT:PSS})]_n$ multilayers during and after catalyzing repeated methanol oxidation are the current focus of the work.

CONCLUSIONS

Polyethylenimine-capped platinum nanoparticles (PEI-capped Pt NPs) were explored as an aqueous dispersed component for layer-by-layer deposition. The photoreduction of hexachloroplatinic acid in the presence of polyethylenimine affords a cationic PEI-capped Pt NPs that electrostatically associate with poly(3,4-ethylenedioxythiophene):poly(*p*-styrenesulfonate)

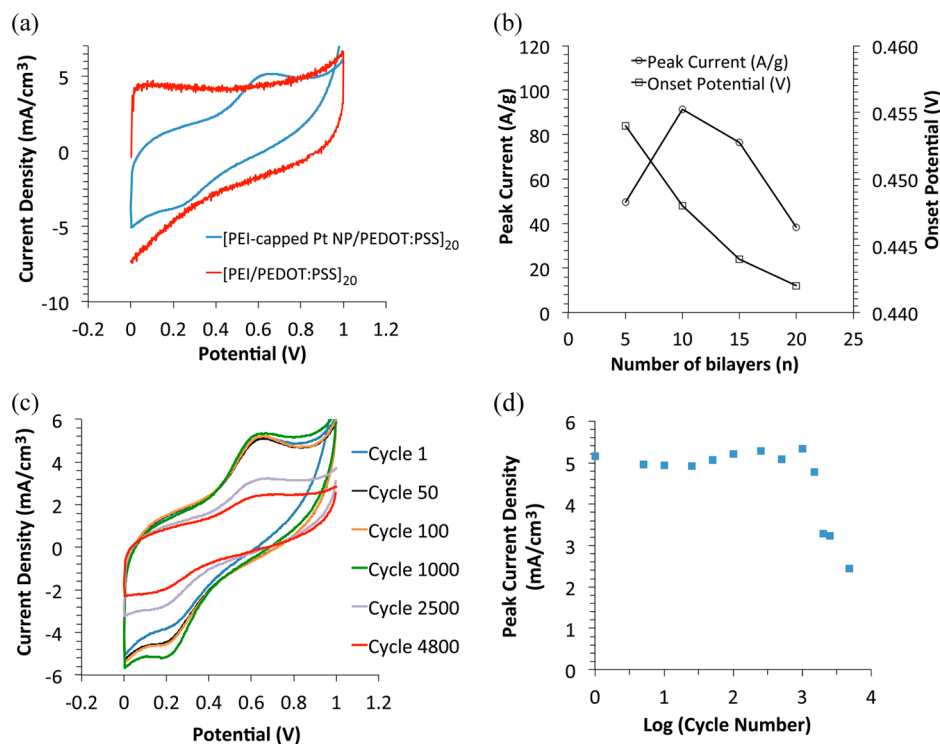


Figure 5. (a) Cyclic voltammetry (vs Ag/AgCl) plots for methanol oxidation reaction catalyzed by a [PEI-capped Pt NPs/(PEDOT:PSS)]₂₀ multilayer working electrode at 0.050 V/sec in 0.1 M H₂SO₄ and 2 M CH₃OH. (b) Peak current and onset potential vs. bilayer number for methanol oxidation catalyzed by [PEI-capped Pt NPs/(PEDOT:PSS)]_n, where $n = 5, 10, 15$, and 20 . (c) Selected voltammograms acquired from a 4800 cyclic voltammetry study using a [PEI-capped Pt NPs/(PEDOT:PSS)]₂₀ multilayer for repeated methanol oxidation reactions. (d) Plot for peak current density value vs log(voltammogram cycle number) from study described in c.

[(PEDOT:PSS)⁻Na⁺]. When these two components are incorporated in an LbL assembly procedure, a controlled deposition of an electrostatically crosslinked multilayer occurs where the coating thickness appears to follow a second-order polynomial type trend. A detailed characterization of the physical and chemical constitution of a series of samples confirms that the resulting multilayers incorporate each component over a wide bilayer number range ($n = 0$ – 20). A 20 bilayer coating was found to be composed with $\sim 12\%$ Pt NPs by mass and as such is catalytically active for the methanol oxidation when supported on an ITO anode. The lifetime of the catalytic activity was evaluated and revealed that a multilayer of this type is capable of a near-constant level of activity for the methanol oxidation reaction for over 1000 cycles. The mechanism for the longevity in the catalytic activity is proposed to result from a constant electroactive Pt surface area because of reduced NP particle diffusion and aggregation within the highly electrostatically crosslinked multilayer.

ASSOCIATED CONTENT

Supporting Information

UV-vis spectra for (PEDOT:PSS)⁻Na⁺ and for the characterization of synthesis of the PEI-capped Pt NPs (Figure S1), zeta potential plots for PEI, H₂PtCl₆-loaded PEI, PEI-capped Pt NPs and (PEDOT:PSS)⁻Na⁺ (Figure S2), optimized conditions used for ICP-MS measurements (Table S1), relative atomic concentration for Pt and S for [PEI-capped Pt NPs/(PEDOT:PSS)]_n multilayer films on ITO estimated by laser ablation ICP-MS (Figure S3), platinum-loading versus bilayer number (Table S2), SFM step-height analysis of [PEI-capped Pt NPs/(PEDOT:PSS)]_n and [PEI/(PEDOT:PSS)]₂₀ multi-

layer films for $n = 0$ – 20 (Figure S4), and Cyclic voltammetry plots for methanol oxidation reaction catalyzed by a (i) [PEI-capped Pt NPs/(PEDOT:PSS)]_n multilayer films on ITO for $n = 5$ – 20 and (ii) a [PEI-capped Pt NPs/(PEDOT:PSS)]₂₀ multilayer films exposed to CO (Figure S5). This material is available free of charge via the Internet at <http://pubs.acs.org>.

AUTHOR INFORMATION

Corresponding Author

*E-mail: david.rider@wwu.edu.

Notes

The authors declare no competing financial interest.

ACKNOWLEDGMENTS

This work was supported by a faculty start-up grant from the Advanced Materials Science and Engineering Center at Western Washington University (AMSEC WWU). Cyclic voltammetry equipment was purchased with funds from an American Chemical Society Petroleum Research Fund, Undergraduate New Investigator Grant (ACS-PRF UNI # 51559-UNI10). K.R.K., C.C.H., A.L.F., and B.W. are grateful for undergraduate research grants from the Vice Provost for Research at WWU. This work made use of 4D LABS shared facilities supported by the Canada Foundation for Innovation (CFI), British Columbia Knowledge Development Fund (BCKDF), Western Economic Diversification Canada, and Simon Fraser University. The authors acknowledge the contributions of Maryam S. Mahmoudi, Amir Nazemi, Brandy Kinkead, and Dr. Byron D. Gates in the Department of Chemistry at Simon Fraser University for their assistance in

dynamic light scattering measurements and electron microscopy, and for their helpful discussions.

■ REFERENCES

- (1) Decher, G. *Science* **1997**, *277*, 1232–1237.
- (2) Decher, G.; Hong, J. D.; Schmitt, J. *Thin Solid Films* **1992**, *210*, 831–835.
- (3) Bertrand, P.; Jonas, A.; Laschewsky, A.; Legras, R. *Macromol. Rapid Commun.* **2000**, *21*, 319–348.
- (4) Hammond, P. T. *Curr. Opin. Colloid Interface Sci.* **1999**, *4*, 430–442.
- (5) Klitzing, R. V. *Phys. Chem. Chem. Phys.* **2006**, *8*, 5012–5033.
- (6) Jaber, J. A.; Schlenoff, J. B. *Curr. Opin. Colloid Interface Sci.* **2006**, *11*, 324–329.
- (7) Ariga, K.; Hill, J. P.; Ji, Q. M. *Phys. Chem. Chem. Phys.* **2007**, *9*, 2319–2340.
- (8) Hammond, P. T. *Adv. Mater.* **2004**, *16*, 1271–1293.
- (9) Azzaroni, O.; Lau, K. H. A. *Soft Matter* **2011**, *7*, 8709–8724.
- (10) Quinn, J. F.; Johnston, A. P. R.; Such, G. K.; Zelikin, A. N.; Caruso, F. *Chem. Soc. Rev.* **2007**, *36*, 707–718.
- (11) Caruso, F. *Colloid Chem. II* **2003**, *227*, 145–168.
- (12) Lutkenhaus, J. L.; Hammond, P. T. *Soft Matter* **2007**, *3*, 804–816.
- (13) Srivastava, S.; Kotov, N. A. *Acc. Chem. Res.* **2008**, *41*, 1831–1841.
- (14) Delcea, M.; Möhwald, H.; Skirtach, A. G. *Adv. Drug Delivery Rev.* **2011**, *63*, 730–747.
- (15) Pingarron, J. M.; Yanez-Sedeno, P.; Gonzalez-Cortes, A. *Electrochim. Acta* **2008**, *53*, 5848–5866.
- (16) Such, G. K.; Johnston, A. P. R.; Caruso, F. *Chem. Soc. Rev.* **2011**, *40*, 19–29.
- (17) Ariga, K.; Ji, Q. M.; Hill, J. P.; Enzyme-Encapsulated Layer-by-Layer Assemblies: Current Status and Challenges Toward Ultimate Nanodevices. In *Modern Techniques For Nano- And Microreactors-Reactions*, Springer-Verlag: Berlin, 2011; Vol. 229, pp 51–87.
- (18) Tokarev, I.; Minko, S. *Soft Matter* **2009**, *5*, 511–524.
- (19) Campas, M.; O'Sullivan, C. *Anal. Lett.* **2003**, *36*, 2551–2569.
- (20) Zhao, W.; Xu, J. J.; Chen, H. Y. *Electroanalysis* **2006**, *18*, 1737–1748.
- (21) Wang, J.; Zhao, C. J.; Lin, H. D.; Zhang, G.; Zhang, Y.; Ni, J.; Ma, W. J.; Na, H. J. *Power Sources* **2011**, *196*, 5432–5437.
- (22) Taylor, A. D.; Michel, M.; Sekol, R. C.; Kizuka, J. M.; Kotov, N. A.; Thompson, L. T. *Adv. Funct. Mater.* **2008**, *18*, 3003–3009.
- (23) Zhang, X.; Zan, X. J.; Su, Z. H. *J. Mater. Chem.* **2011**, *21*, 17783–17789.
- (24) Crespiho, F. N.; Zucolotto, V.; Oliveira, O. N.; Nart, F. C. *Int. J. Electrochem. Sci.* **2006**, *1*, 194–214.
- (25) Zhao, T. S.; Chen, R.; Yang, W. W.; Xu, C. *J. Power Sources* **2009**, *191*, 185–202.
- (26) Yu, X. W.; Pickup, P. G. *J. Power Sources* **2008**, *182*, 124–132.
- (27) Tang, Z. C.; Lu, G. X. *Prog. Chem.* **2007**, *19*, 1301–1312.
- (28) Fuel Cell System Cost for Transportation—2008 Cost Estimate. In *U.S. Department of Energy Hydrogen Program*; U.S. Department of Energy: Washington, DC, 2009; 62 p.
- (29) Serov, A.; Kwak, C. *Appl. Catal., B* **2009**, *90*, 313–320.
- (30) Antolini, E. *J. Power Sources* **2007**, *170*, 1–12.
- (31) Arico, A. S.; Srinivasan, S.; Antonucci, V. *Fuel Cells* **2001**, *1*, 133–161.
- (32) Ren, Z. B.; Wang, H. L.; Cai, Y. Q.; Chen, M.; Qian, D. J. *Mater. Chem. Phys.* **2011**, *127*, 310–315.
- (33) Ahmed, M.; Dincer, I. *Int. J. Energy Res.* **2011**, *35*, 1213–1228.
- (34) Liu, H. S.; Song, C. J.; Zhang, L.; Zhang, J. J.; Wang, H. J.; Wilkinson, D. P. *J. Power Sources* **2006**, *155*, 95–110.
- (35) Deligoz, H.; Yilmazturk, S.; Karaca, T.; Ozdemir, H.; Koc, S. N.; Oksuzomer, F.; Durmus, A.; Gurkaynak, M. A. *J. Membr. Sci.* **2009**, *326*, 643–649.
- (36) Vercelli, B.; Zotti, G.; Berlin, A. *J. Phys. Chem. C* **2009**, *113*, 3525–3529.
- (37) Pandey, R. K.; Lakshminarayanan, V. *J. Phys. Chem. C* **2010**, *114*, 8507–8514.
- (38) Tsakova, V.; Ivanov, S.; Lange, U.; Stoyanova, A.; Lyutov, V.; Mirsky, V. M. *Pure Appl. Chem.* **2011**, *83*, 345–358.
- (39) Patten, H. V.; Ventosa, E.; Colina, A.; Ruiz, V.; Lopez-Palacios, J.; Wain, A. J.; Lai, S. C. S.; Macpherson, J. V.; Unwin, P. R. J. *Solid State Electrochem.* **2011**, *15*, 2331–2339.
- (40) Kidambi, S.; Bruening, M. L. *Chem. Mater.* **2005**, *17*, 301–307.
- (41) Dotzauer, D. M.; Dai, J. H.; Sun, L.; Bruening, M. L. *Nano Lett.* **2006**, *6*, 2268–2272.
- (42) Farhat, T. R.; Hammond, P. T. *Chem. Mater.* **2006**, *18*, 41–49.
- (43) Cho, S. J.; Ouyang, J. Y. *J. Phys. Chem. C* **2011**, *115*, 8519–8526.
- (44) Wang, S. J.; Choi, Y. J.; Park, H. H. *Ceram. Int.* **2012**, *38*, S453–S456.
- (45) Bai, L. T.; Zhu, H. Z.; Thrasher, J. S.; Street, S. C. *ACS Appl. Mater. Interfaces* **2009**, *1*, 2304–2311.
- (46) Suh, J.; Paik, H. J.; Hwang, B. K. *Bioorg. Chem.* **1994**, *22*, 318–327.
- (47) Porcel, C.; Lavalle, P.; Ball, V.; Decher, G.; Senger, B.; Voegel, J. C.; Schaaf, P. *Langmuir* **2006**, *22*, 4376–4383.
- (48) Peng, C. Q.; Thio, Y. S.; Gerhardt, R. A.; Ambaye, H.; Lauter, V. *Chem. Mater.* **2011**, *23*, 4548–4556.
- (49) Lutkenhaus, J. L.; McEnnis, K.; Hammond, P. T. *Macromolecules* **2008**, *41*, 6047–6054.
- (50) Li, S. K.; Zhang, L.; Huang, F. Z.; Yu, X. R.; Xie, A. J.; Shen, Y. H.; Wang, Y. *Thin Solid Films* **2011**, *519*, 5609–5615.
- (51) Xie, H.; Gu, Y. L.; Ploehn, H. J. *Nanotechnology* **2005**, *16*, S492–S501.
- (52) Cameron, R. E.; Bocarsly, A. B. *Inorg. Chem.* **1986**, *25*, 2910–2913.
- (53) Agarwal, M.; Lvov, Y.; Varahramyan, K. *Nanotechnology* **2006**, *17*, 5319–5325.
- (54) Sakamoto, Y.; Fukuoka, A.; Higuchi, T.; Shimomura, N.; Inagaki, S.; Ichikawa, M. *J. Phys. Chem. B* **2003**, *108*, 853–858.
- (55) Radziuk, D.; Möhwald, H.; Shchukin, D. *J. Phys. Chem. C* **2008**, *112*, 19257–19262.
- (56) Rider, D. A.; Worfolk, B. J.; Harris, K. D.; Lalany, A.; Shahbazi, K.; Fleischauer, M. D.; Brett, M. J.; Buriak, J. M. *Adv. Funct. Mater.* **2010**, *20*, 2404–2415.
- (57) Dawidczyk, T. J.; Walton, M. D.; Jang, W. S.; Grunlan, J. C. *Langmuir* **2008**, *24*, 8314–8318.
- (58) DeLongchamp, D.; Hammond, P. T. *Adv. Mater.* **2001**, *13*, 1455–1459.
- (59) Lin, Y. J.; Li, Y. C.; Yeh, H. J.; Wang, Y. H.; Wen, T. C.; Huang, L. M.; Chen, Y. K. *Appl. Phys. Lett.* **2007**, *91* (253501), 1–3.
- (60) Picart, C.; Mutterer, J.; Richert, L.; Luo, Y.; Prestwich, G. D.; Schaaf, P.; Voegel, J.-C.; Lavalle, P. *Proc. Natl. Acad. Sci. U.S.A.* **2002**, *99*, 12531–12535.
- (61) Yoo, P. J.; Nam, K. T.; Qi, J.; Lee, S.-K.; Park, J.; Belcher, A. M.; Hammond, P. T. *Nat. Mater.* **2006**, *5*, 234–240.
- (62) Ostrander, J. W.; Mamedov, A. A.; Kotov, N. A. *J. Am. Chem. Soc.* **2001**, *123*, 1101–1110.
- (63) Schmitt, J.; Decher, G.; Dressick, W. J.; Brandow, S. L.; Geer, R. E.; Shashidhar, R.; Calvert, J. M. *Adv. Mater.* **1997**, *9*, 61–65.
- (64) Bayer, Baytron P Product Information.
- (65) Habibi, B.; Pournaghi-Azar, M. H. *Int. J. Hydrogen Energy* **2010**, *35*, 9318–9328.
- (66) Huang, J. H.; Chu, C. W. *Electrochim. Acta* **2011**, *56*, 7228–7234.
- (67) Avila-Garcia, I.; Ramirez, C.; Lopez, J. M. H.; Estrada, E. M. A. *J. Alloys Compd.* **2010**, *495*, 462–465.
- (68) Neto, A. O.; Perez, J.; Napporn, W. T.; Ticianelli, E. A.; Gonzalez, E. R. *J. Braz. Chem. Soc.* **2000**, *11*, 39–43.
- (69) Crespiho, F. N.; Huguenin, F.; Zucolotto, V.; Olivi, P.; Nart, F. C.; Oliveira, O. N. *Electrochim. Commun.* **2006**, *8*, 348–352.
- (70) Goodenough, J. B.; Hamnett, A.; Kennedy, B. J.; Manoharan, R.; Weeks, S. A. *J. Electroanal. Chem.* **1988**, *240*, 133–145.
- (71) Rhee, C. K.; Kim, B.-J.; Ham, C.; Kim, Y.-J.; Song, K.; Kwon, K. *Langmuir* **2009**, *25*, 7140–7147.

(72) Şen, F.; Gökağaç, G. *J. Phys. Chem. C* **2007**, *111*, 1467–1473.
(73) A preliminary demonstration of the resiliency of the catalytic activity of [PEI-capped Pt NPs/(PEDOT:PSS)]_n multilayers to CO poisoning is included in the Supporting Information. Briefly, the peak current density for the electrocatalysis of methanol oxidation by [PEI-capped Pt NPs/(PEDOT:PSS)]₂₀ after a 2 h exposure to 1 atm of CO was approximately equal to that of the unexposed multilayer.